

## Article

# Design of a Dynamic Hybrid Compensator for Current Sharing Control of Parallel Phase-Shifted Full-Bridge Converter

Baihui Gong<sup>1</sup>, Kan Liu<sup>1,\*</sup>, Haozhe Luan<sup>1,\*</sup>, Jiaming Wu<sup>1</sup>, Jing Zhou<sup>1</sup>, Shilin Tan<sup>1</sup>, Chao Huang<sup>1</sup> and Huajiang Wu<sup>2</sup>

<sup>1</sup> College of Mechanical and Vehicle Engineering, Hunan University, Changsha 410000, China

<sup>2</sup> Ningbo Anson CNC Technique Co., Ltd., Ningbo 315000, China

\* Correspondence: lkan@hnu.edu.cn (K.L.); luanhz@hnu.edu.cn (H.L.)

**Abstract:** The phase-shifted full-bridge (PSFB) converter has been widely used in power supply modules due to its simple control and high output power. However, with the market's increasing demand for higher power sources, the PSFB converter needs to face challenges in increasing its output power level. Compared to redesigning a larger power module or a larger single converter, it will be more cost-effective to achieve a higher power output by paralleling the existing converters. However, due to the manufacturing differences in circuit components, the output imbalance in parallel PSFB converter systems may damage the power modules. Thus, the influence of differences in circuit components is analyzed in this paper, and it is found that the leakage inductance and transformer ratio are the main factors resulting in errors in current sharing control. Consequently, a dynamic hybrid compensator (DHC) is proposed in this paper, that can significantly reduce the error in current sharing control via the compensation of the duty cycle of a slave module. Furthermore, the DHC is verified on an 800 W two-phase PSFB converter, which shows that even when the difference in components is as large as 20%, the proposed method can still reduce the error in current sharing control to less than 2% under both half and full load conditions.

**Keywords:** current sharing control; parallel PSFB; dynamic hybrid compensator



**Citation:** Gong, B.; Liu, K.; Luan, H.; Wu, J.; Zhou, J.; Tan, S.; Huang, C.; Wu, H. Design of a Dynamic Hybrid Compensator for Current Sharing Control of Parallel Phase-Shifted Full-Bridge Converter. *Energies* **2023**, *16*, 2204. <https://doi.org/10.3390/en16052204>

Academic Editors: Matej Zajc, Hugo Morais and Junjie Hu

Received: 24 December 2022

Revised: 21 February 2023

Accepted: 22 February 2023

Published: 24 February 2023



**Copyright:** © 2023 by the authors. Licensee MDPI, Basel, Switzerland. This article is an open access article distributed under the terms and conditions of the Creative Commons Attribution (CC BY) license (<https://creativecommons.org/licenses/by/4.0/>).

## 1. Introduction

Power demand is increasing in areas such as electric vehicle charging, photovoltaic power stations and communication base station equipment. The PSFB converter is one of the most widely used circuits in these areas. Therefore, the market's demand for a high output power PSFB converter has increased in recent years. Compared to redesigning a larger power module or a larger single converter, using existing power modules to achieve larger power levels through series-parallel output can be more cost-effective while also reducing carbon emissions and achieving environmental protection. There are four main types of power modules connection [1]: input-series output-series (ISOS), input-series output-parallel (ISOP), input-parallel output-series (IPOS) and input-parallel output-parallel (IPOP). Series connection can reduce the voltage load on each power module [2] and parallel connection can expand the power level [3]. Each connection type has its own application situation and characteristic. Input-side and output-side voltage and current characteristics for these connection types are shown in Table 1 [4,5].

IPOP connection can reduce the current stress on each module by distributing the total power between different power modules. Thus, the size of magnetic circuit components (transformers and inductors) can be reduced [6]. Furthermore, IPOP can improve the thermal distribution and lead to greater system reliability [7]. In a multiphase power converter system, each phase is designed to be the same. In reality, manufacturing differences, environmental changes and other factors usually lead to an inconsistent output current [8]. The presence of circuit component manufacturing differences will cause power imbalances

among modules, thereby leading to thermal stress imbalances, inductor saturation and performance reduction [9]. In severe cases, the component differences may result in an excessive power burden on some modules while others have only a small power output [10]. In [11], the IPOPOP-LLC system manufacturing differences influences are researched.

**Table 1.** Characteristics of different connection types.

Connection Type	Application Situation	Input Side Characteristics	Output Side Characteristics
ISOS	High input and output voltage	voltage imbalance and current equalization	voltage imbalance and current equalization
ISOP	Converting from high voltage to low voltage	voltage imbalance and current equalization	voltage equalization and current imbalance
IPOS	Converting from low voltage to high voltage	voltage equalization and current imbalance	voltage imbalance and current equalization
IPOP	Power expansion	voltage equalization and current imbalance	voltage equalization and current imbalance

There are two main ways to achieve current sharing: one is through control algorithms and the other is through changing the circuit structure. For the control algorithm, the common duty ratio control is one of the most used current sharing control algorithms. It is applied in the forward converter and dual active bridge (DAB) converter, respectively, to improve the current imbalance in [12,13]. However, the output current sharing error is still large when the IPOPOP-PSFB converter has a large transformer ratio difference. A current sensorless parameter estimation and current equalization control strategy is proposed in [14], which considers the effect of transformer difference on the current sharing error of the IPOPOP-DAB converter. Simultaneously, it is also proved to be the main cause of the parallel PSFB current imbalance.

In [15,16], the automatic current sharing control of two-phase LLC is realized via changing the circuit structure of the traditional LLC without the addition of a current sharing control algorithm. The IPOPOP-LLC system's excellent current sharing performances are addressed by using a common inductor [15] and common capacitor [16]. The load coefficient  $k$  is introduced in the LLC converter [17,18] and the buck converter [19] to measure the output power balance of each phase power module.

PSFB has the characteristics of simple control, wide voltage adjustment range and high output power [20]. A saturable inductor [21] and clamping diodes [22] are applied in PSFB to reduce duty cycle loss. To meet the requirement of different applications, multi-phase PSFBs have been studied. A new connection method for output filter capacitors is proposed in [23], which is applied to the IPOS-PSFB converter to achieve output voltage balancing. A new circuit is proposed in [24], which uses a blocking capacitor and hybrid rectifier diodes in ISOP-PSFB to achieve zero-voltage and zero-current switching of the primary-side switches. Meanwhile, the output current imbalance has also been reduced by the circuit. Common duty ratio control is also applied in ISOP-PSFB; all phases are controlled by the same duty ratio [25]. However, the literature on IPOPOP-PSFB converter is still not thorough enough.

In this paper, it is found that the circuit parameters contribute different influences to the error of current sharing control, of which the transformer difference has the greatest impact on the output power imbalance. To mitigate the current imbalance, a dynamic hybrid compensator (DHC) for achieving the current sharing control of the IPOPOP-PSFB converter is proposed. The compensator can reduce the error of current sharing control via a phase-shift duty cycle compensation of the slave module. The proposed method can control the error of current sharing control in real time and still retain a good performance in maintaining the current balance even when the difference in components is as large as 20% in each phase circuit component.

The rest of this paper is presented as follows. In Section 2, the single phase PSFB gain equation, considering the duty cycle loss, is derived. In Section 3, the mathematical model analyzes the effect of different types of component differences on output power imbalance. Additionally, a dynamic hybrid compensator (DHC) is designed to achieve the error reduction of current sharing control. The feasibility of proposed DHC is verified by both simulation and experiments in Sections 4 and 5, respectively.

### 2. Derivation of PSFB Gain Equation Considering Duty Cycle Loss

In this section the PSFB voltage gain equation, considering the duty cycle loss problem, is derived. The switching singles and waveform of the PSFB are shown in Figure 1. The PSFB converter is shown in Figure 2. Figure 1 shows that during the  $t_0 \sim t_1$  and  $t_2 \sim t_3$ , the duty cycle of the transformer’s primary side voltage  $V_p$  and secondary side voltage  $V_s$  is less than the duty cycle of the converter arm voltage  $V_{AB}$ .  $D$  is the duty cycle of  $V_{AB}$ ;  $D_{eff}$  is the duty cycle of  $V_p$  and  $V_s$ ;  $D_{loss}$  is the loss of duty cycle;  $T_s$  is the switching cycle;  $I_p$  (1) and  $I_p$  (2) are the primary side current at  $t_0$  and  $t_1$  respectively;  $I_f$  is the current of filter inductor;  $I_o$  is output current, equal to the average of  $I_f$ . and  $I_D$  is the current of the rectifier diode.

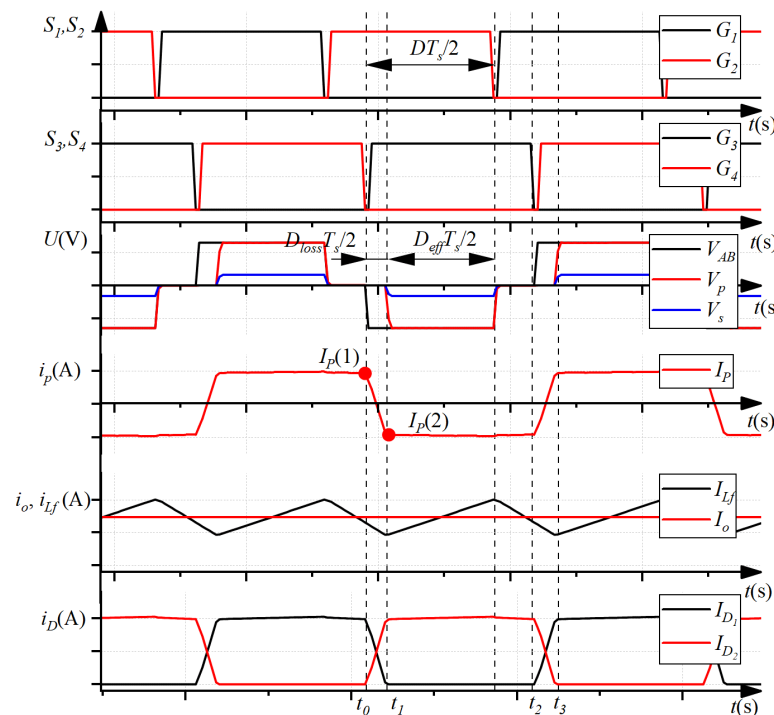


Figure 1. Switching singles and key waveform of PSFB.

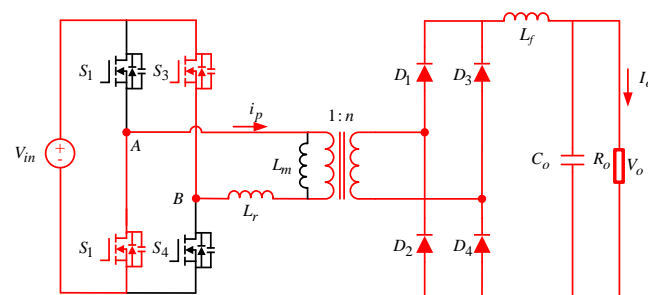


Figure 2. Operation mode during  $t_0 \sim t_1$ .

Figure 2 shows the operation mode during  $t_0 \sim t_1$ ; the operation mode of  $t_2 \sim t_3$  is symmetrical. In these operation modes, the commutation of the primary side current

occurs and the current on the primary side gradually rises to the load current. Although  $V_{AB}$  is not equal to 0, the primary side voltage  $V_p$  is equal to 0. This is because the primary side current  $I_p$  is changing direction and the current converted to the secondary side is less than the  $I_o$ . This results in the  $I_o$  needing to be renewed through the  $I_f$  and the output rectifier bridge upper and lower tubes conduct at the same time. Thus, the secondary winding is shorted, the voltage of the secondary winding is clamped to zero and the voltage of the primary side will also be clamped at zero. So, compared to  $V_{AB}$ ,  $V_p$  and  $V_s$  loses the voltage waveform. This phenomenon leads to a reduction in the effective duty cycle.

$$D_{eff} = D - D_{loss} \tag{1}$$

The loss of duty cycle during voltage clamping of transformer windings is shown in Figure 3. During this time, the relationship between the voltage and current of the primary leakage inductor is:

$$V_{in} = \frac{L_r(I_p(1) - I_p(2))}{T_s D_{loss} / 2} \tag{2}$$

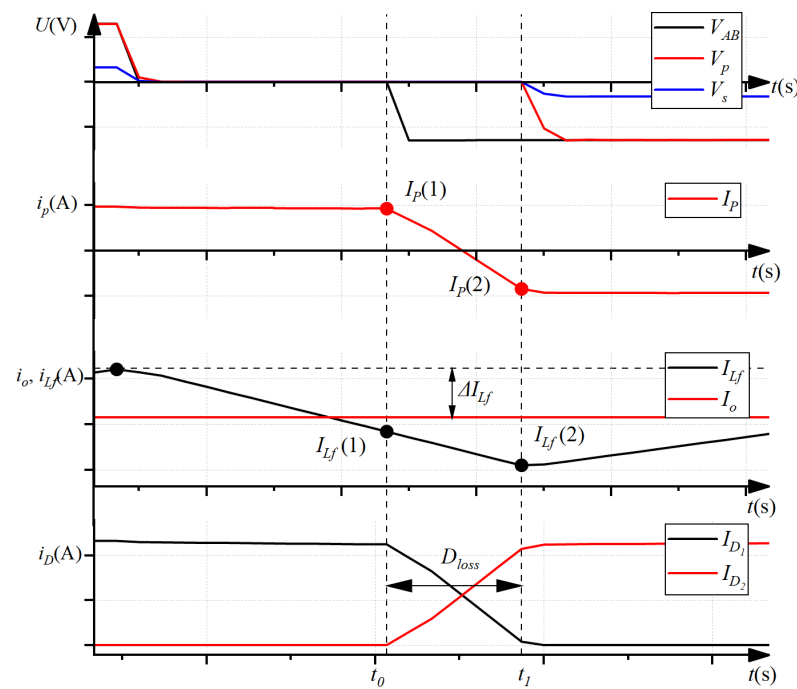


**Figure 3.** Loss of duty cycle during voltage clamping of transformer windings.

The relationship between the primary side current  $I_p(1)$ ,  $I_p(2)$  and the secondary filter inductor current  $I_{Lf}(1)$ ,  $I_{Lf}(2)$  is:

$$\begin{cases} I_p(1) = nI_{Lf}(1) \\ I_p(2) = -nI_{Lf}(2) \end{cases} \tag{3}$$

where  $n$  is the transformer turns ratio of the secondary side to the primary side.

The filter inductor current  $I_{Lf}(1)$ ,  $I_{Lf}(2)$  can be expressed as

$$\begin{cases} I_{Lf}(1) = I_o + \Delta I_{Lf} - \frac{V_o(1-D)}{L_f} \cdot \frac{T_s}{2} \\ I_{Lf}(2) = I_o - \Delta I_{Lf} \end{cases} \tag{4}$$

where  $\Delta I_{Lf}$  is the fluctuation of filter inductor current;  $I_o$  is the average current of filter inductor, equal to the output current;  $V_o$  is the output voltage and  $L_f$  is the output filter inductor value.

Combining Equations (2)–(4), the loss of duty cycle can be calculated as:

$$D_{loss} = \frac{nL_r [4L_f I_o f_s - V_o(1-D)]}{V_{in} L_f} \quad (5)$$

Substituting Equation (5) into Equation (1), the expression for the effective duty cycle can be rewritten as:

$$D_{eff} = D - \frac{4n^2 I_o L_r f_s - n^2 V_o L_x (1-D)}{nV_{in}} \quad (6)$$

where  $L_x = \frac{L_r}{L_f}$ .

Ignoring diode voltage drop, the relationship between the input voltage and output voltage can be obtained by integrating the output voltage of the secondary rectifier bridge:

$$V_o = \int_0^{T_s} D_{eff} T_s V_s dt = D_{eff} V_s = D_{eff} nV_{in} \quad (7)$$

Combining Equations (6) and (7) can obtain the PSFB gain equation:

$$G = \frac{V_o}{V_{in}} = \frac{nD}{1 + 4n^2 L_r f_s / R - n^2 L_x (1-D)} \quad (8)$$

### 3. Analysis of Parallel PSFB Converter

Circuit component manufacturing differences will result in a severe load current imbalance and impair the performance of the parallel structure with the multiphase PSFB converter. The definitions of the parameters are provided in Section 3.1. The influence of each component difference on the performance of current sharing control of a parallel PSFB system is analyzed in Section 3.2. The design of the DHC for current sharing control of a parallel PSFB converter system is introduced in Section 3.3.

#### 3.1. Two-Phase Parallel PSFB Converter

Figure 4 shows an input-parallel-output-parallel two-phase PSFB converter.

$S_{1,1}$ ,  $S_{1,2}$ ,  $S_{1,3}$ ,  $S_{1,4}$  and  $S_{2,1}$ ,  $S_{2,2}$ ,  $S_{2,3}$ ,  $S_{2,4}$  are the primary switches of phase #1 and phase #2, respectively.  $D_{1,1}$ ,  $D_{1,2}$ ,  $D_{1,3}$ ,  $D_{1,4}$  and  $D_{2,1}$ ,  $D_{2,2}$ ,  $D_{2,3}$ ,  $D_{2,4}$  are the rectifier diodes on the secondary side of the two phases.

$L_{r1}$ ,  $L_{m1}$  and  $L_{f1}$  are the primary leakage inductor, primary magnetizing inductor and secondary filter inductor of phase #1, respectively.  $L_{r2}$ ,  $L_{m2}$  and  $L_{f2}$  are the primary leakage inductor, primary magnetizing inductor, and secondary filter inductor of phase #2, respectively.  $n_1$  and  $n_2$  are the ratio of turns of the secondary side to the primary side coil of phase #1 and phase #2, respectively.  $V_{in}$  is the DC input voltage.  $I_{o1}$ , and  $I_{o2}$  are the load current of the two phases, respectively.  $I_o$  is the total load current.  $R_o$  is the total load resistor.  $V_o$  is the DC output voltage.

During the production process, the manufacturing difference of the components will not exceed  $\pm 10\%$ ; this is considered qualified. Thus, it is assumed that the difference of the two phases' corresponding circuit components is 20% in this paper. The opposite difference directions ( $L_{r1} = 1.2L_{r2}$  and  $L_{r2} = 1.2L_{r1}$ ) lead to the same current sharing error, despite the current distribution being opposite. Parameters  $a$ ,  $b$ , and  $c$  show that the circuit hardware parameters of the two phases are different from each other. The circuit component values of the two phases can be defined as:

$$\begin{cases} L_{r1} = L_r, & L_{r2} = aL_r \\ L_{f1} = L_f, & L_{f2} = bL_f \\ n_1 = n, & n_2 = cn \end{cases} \quad (9)$$

$P_o$  is the total output power. The  $R_o$  can be expressed as:

$$R_o = \frac{V_o^2}{P_o} \tag{10}$$

$P_{o1}$  and  $P_{o2}$  are the power generated by the two phases. The relationship between  $P_{o1}$ ,  $P_{o2}$  and  $P_o$  is:

$$P_o = P_{o1} + P_{o2} \tag{11}$$

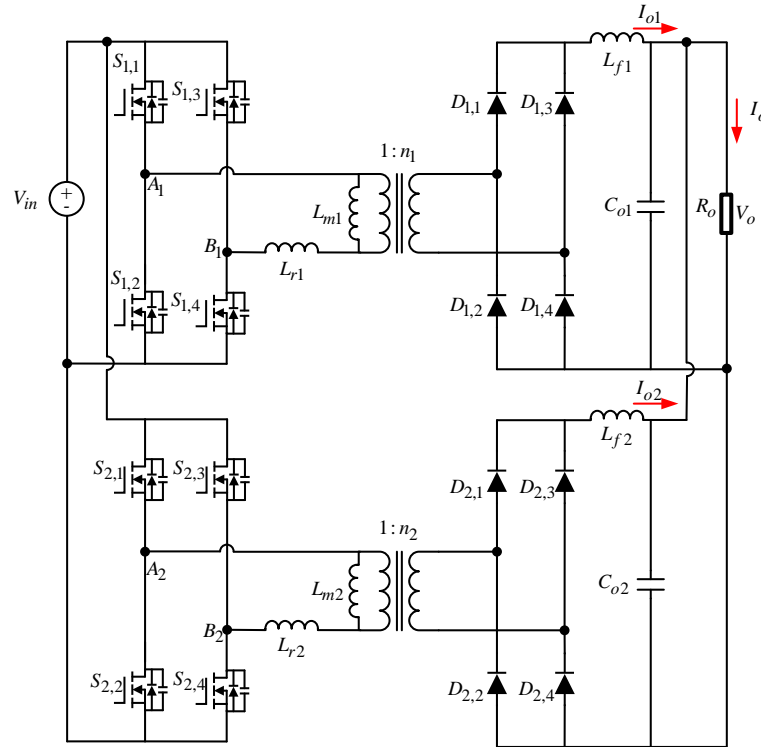


Figure 4. Two-phase parallel PSFB converter.

The equivalent load resistors  $R_{o1}$  and  $R_{o2}$  of each phase can be expressed as:

$$\begin{cases} R_{o1} = \frac{V_o^2}{P_{o1}} \\ R_{o2} = \frac{V_o^2}{P_{o2}} \end{cases} \tag{12}$$

Defining  $k$  as the ratio of the load power generated by phase#1 [18], the  $P_{o1}$  and  $P_{o2}$  can be described as:

$$\begin{cases} P_{o1} = kP_o \\ P_{o2} = (1 - k)P_o \end{cases} \tag{13}$$

Combine Equations (11)–(13):

$$[R_{o1} \quad R_{o2}] = \begin{cases} \begin{bmatrix} \infty & R_o \end{bmatrix} & k \leq 0 \\ \begin{bmatrix} \frac{R_o}{k} & \frac{R_o}{1-k} \end{bmatrix} & 0 < k < 1 \\ \begin{bmatrix} R_o & \infty \end{bmatrix} & k \geq 1 \end{cases} \tag{14}$$

When  $k \leq 0$ , phase #2 will supply all the power, and the phase #1 equivalent load resistor  $R_{o1}$  will become infinite. When  $0 < k < 1$ , each phase will supply part of the total power.

Define the current sharing error  $\sigma_{load}$  to evaluate the current sharing capability.

$$\sigma_{load} = \left| \frac{I_{o1} - I_{o2}}{I_{o1} + I_{o2}} \right| = |2k - 1| \quad (15)$$

If  $\sigma_{load} = 0$ , it means that each module has the same output current and both supply half of the total power. If  $\sigma_{load} = 1$  it means there is only one phase to supply all the power.

When using common duty cycle control, according to Equation (8), the two phase PSFB gain can be calculated as:

$$\begin{cases} G_1 = \frac{n_1 D}{1 + 4n_1^2 L_r f_s / R_{o1} - n_1^2 L_{x1} (1 - D)} \\ G_2 = \frac{n_2 D}{1 + 4n_2^2 L_r f_s / R_{o2} - n_2^2 L_{x2} (1 - D)} \end{cases} \quad (16)$$

where  $L_{x1} = \frac{L_{r1}}{L_{f1}}$ ,  $L_{x2} = \frac{L_{r2}}{L_{f2}}$ .

Since the two power modules are connected in input parallel and output parallel, the voltage gain will be the same in the steady state. The relationship is:

$$G_1 = G_2 \quad (17)$$

Combining Equations (14)–(17), the  $k$  can be calculated by:

$$\frac{4n^2 L_r f_s}{R_o} (1 + ac)k = \frac{1}{c} - 1 + \frac{4n^2 L_r f_s}{R_o} ac + n^2 \frac{L_r}{L_f} [(1 - D) - c \frac{a}{b} (1 - D)] \quad (18)$$

To analyze the current sharing control performance, a set of PSFB converter component values are designed and shown in Table 2. The output power is 400 W per phase.

**Table 2.** Values of PSFB-related parameters.

Parameter	Value
Rated input voltage $V_{in}$	200 V
Leakage inductor $L_r$	30 $\mu$ H
Filter inductor $L_f$	200 $\mu$ H
Transformer ratio $1/n$	24:6
Rated output voltage $V_o$	40 V
Total output power $P_o$	half 400 W, total 800 W
Switch frequency	100 kHz

When  $P_o = 400$  W,  $R_o = 4$   $\Omega$ ;  $P_o = 600$  W,  $R_o = 2.667$   $\Omega$ ;  $P_o = 800$  W,  $R_o = 2$   $\Omega$ .

### 3.2. Relationship between Component Difference and $k$

Assume that the component values of the two phases are identical except for the leakage inductors. When  $b = 1$  and  $c = 1$ , considering the relationship between  $a$  and  $k$ , Equation (18) can be calculated as:

$$\frac{4n^2 L_r f_s}{R_o} (1 + a)k = \frac{4n^2 L_r f_s}{R_o} a + n^2 \frac{L_r}{L_f} [(1 - D) - a(1 - D)] \quad (19)$$

Equation (19) can be simplified as:

$$k = \frac{a}{1 + a} + \frac{R_o}{4L_f f_s} \frac{(1 - D)(1 - a)}{1 + a} \quad (20)$$

The solutions of  $k$  for different values of  $a$  at different output power are shown in Figure 5. The value of  $k$  becomes larger as  $a$  becomes larger. But the value of  $k$  changing with  $R_o$  is so small that it can be ignored. In the worst case, ( $a = 1.2$ ),  $k = 0.545$  and the load current sharing error  $\sigma_{load} = 9\%$ .

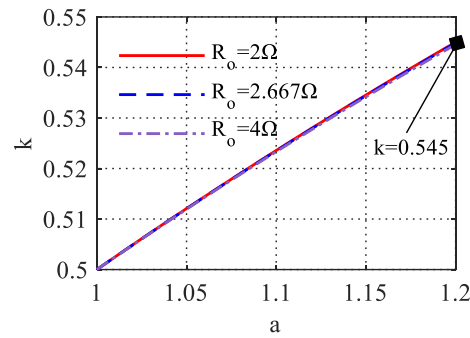


**Figure 5.** Solutions of  $k$  for different values of  $a$  at different output resistances (when  $R_o = 4 \Omega$ ,  $P_o = 400 \text{ W}$ ;  $R_o = 2.667 \Omega$ ,  $P_o = 600 \text{ W}$ ;  $R_o = 2 \Omega$ ,  $P_o = 800 \text{ W}$ ).

When  $a = 1$  and  $c = 1$ , only considering the effect of  $b$  on  $k$ :

$$\frac{8n^2L_r f_s}{R_o} k = \frac{4n^2L_r f_s}{R_o} + n^2 \frac{L_r}{L_f} \left[ (1 - D) - \frac{1}{b}(1 - D) \right] \tag{21}$$

Equation (21) can be simplified as:

$$k = \frac{1}{2} + \frac{R_o}{8L_f f_s} (1 - D) \left( 1 - \frac{1}{b} \right) \tag{22}$$

Figure 6 displays the solutions of  $k$  for various values of  $b$  at various output powers. The value of  $k$  is proportional to  $b$ . As the output power decreases, the value of  $k$  increases. However, even in the worst case ( $b = 1.2$ ,  $R_o = 4 \Omega$ ), the value of  $k = 0.50082$  and  $\sigma_{load} = 0.164\%$ . Compared to the current sharing error caused by other circuit parameters, the error caused by the filter inductor difference is so small as to be negligible. Therefore, in the later part of the analysis, the effect of filter inductor difference can be ignored, meaning  $b = 1$ .

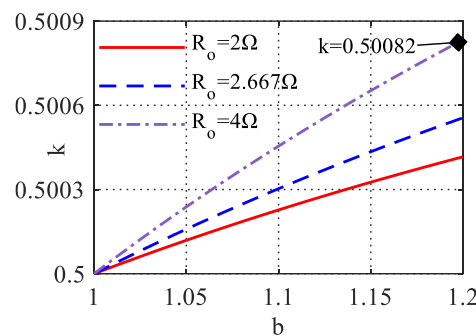


**Figure 6.** Solutions of  $k$  for different values of  $b$  at different output resistances.

When considering only the effect of the transformer ratio difference on  $k$ , Equation (18) can be calculated as:

$$\frac{4n^2L_r f_s}{R_o} (1 + c)k = \frac{1}{c} - 1 + \frac{4n^2L_r f_s}{R_o} c + n^2 \frac{L_r}{L_f} [(1 - D) - c(1 - D)] \tag{23}$$

Equation (23) can be simplified as:

$$k = \frac{1 - c}{c(1 + c)} \frac{R_o}{4n^2L_r f_s} + \frac{c}{1 + c} + \frac{R_o}{4L_f f_s} \frac{1 - c}{1 + c} (1 - D) \tag{24}$$

Figure 7 shows the solution of  $k$  for different output power when the transformer difference increases. When the forward error of transformer ratio difference increases, phase #1 supplies less power. With the total output power decreases, a worse load current imbalance will happen. In the worst case ( $c = 1.2$ ,  $R_o = 4 \Omega$ ),  $k = 0.1405$ , phase #1 only supplies 14.05% of the total power output and  $\sigma_{load} = 71.9\%$ .

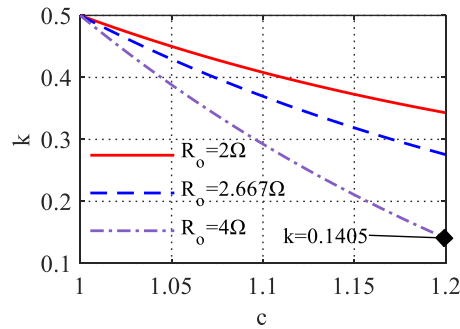


Figure 7. Solutions of  $k$  for different values of  $c$  at different output resistances.

3.3. Designs of a Dynamic Hybrid Compensator for Current Sharing Control of Parallel PSFB

From the above analysis, the impact on the current sharing error on filter inductor difference is minimal, and the ratio difference is the major influencing factor.

Define phase #1 as the master module, and phase#2 as the slave module. Introducing a phase shift duty cycle compensation,  $d$ , the relationship between the master module phase shift duty cycle  $D_1$  and the slave module phase shift duty cycle  $D_2$  is:

$$D_2 = dD_1 = dD \tag{25}$$

Equation (16) becomes:

$$\begin{cases} G_1 = \frac{n_1 D}{1 + 4n_1^2 L_r f_s / R_{o1} - n_1^2 L_{x1} (1 - D)} \\ G_2 = \frac{n_2 d D}{1 + 4n_2^2 L_r f_s / R_{o2} - n_2^2 L_{x2} (1 - D)} \end{cases} \tag{26}$$

When  $k = 0.5$ , each phase provides half of the total power. When  $b = 1$ ,  $k = 0.5$ , Equation (26) can be expressed as:

$$\frac{2n^2 L_r f_s}{R_o} d + \frac{2n^2 L_r f_s}{R_o} ac = \frac{1}{c} - d + \frac{4n^2 L_r f}{R_o} ac + n^2 \frac{L_r}{L_f} [d(1 - D) - ac(1 - dD)] \tag{27}$$

Equation (27) can be simplified as:

$$d + \frac{R_o}{2n^2 L_r f_s} d + \frac{R_o}{2L_f f_s} (ac - acdD - d + dD) = ac + \frac{R_o}{2n^2 c L_r f_s} \tag{28}$$

Thus, the expression of  $d$  is:

$$d = \frac{ac + \frac{R_o}{c\delta} - \frac{acR_o}{2L_f f_s}}{1 + \frac{R_o}{\delta} - \frac{R_o(acD - D + 1)}{2L_f f_s}} \tag{29}$$

where  $\delta = 2n^2 L_r f_s$ . Figure 8 shows the solution of  $d$ .

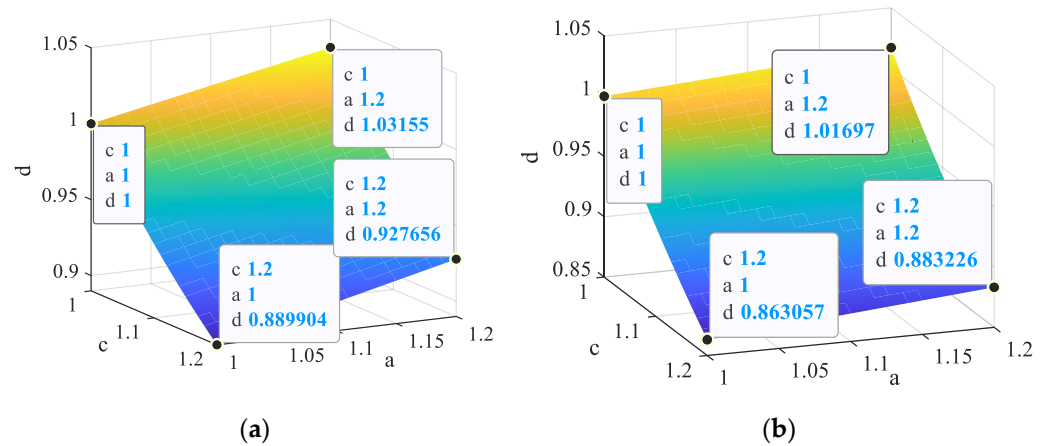


**Figure 8.** Solution of phase shift duty cycle compensation  $d$  in different output resistances: (a)  $R_o = 2 \Omega$ ,  $P_o = 800 \text{ W}$ ; (b)  $R_o = 4 \Omega$ ,  $P_o = 400 \text{ W}$ .

In the PSFB converter, the filter inductor is generally at the  $\mu\text{H}$  level and the switching frequency can reach 50 kHz or more. This causes the factor  $R_o(ac - acdD - d + dD) / (2L_f f_s)$  to become so small that it can be ignored. After simplifying, the expression of  $d$  becomes:

$$d = \frac{ac + \frac{R_o}{c\delta}}{1 + \frac{R_o}{\delta}} \tag{30}$$

Figure 9 shows the solution of  $d$  according to Equation (30). Figure 10 shows the error of  $d$  for the solution of Equation (30). The biggest error is 0.0021 when  $a = 1.2$ ,  $c = 1.2$  and  $R_o = 4 \Omega$ , so  $d$  can be calculated by Equation (30).

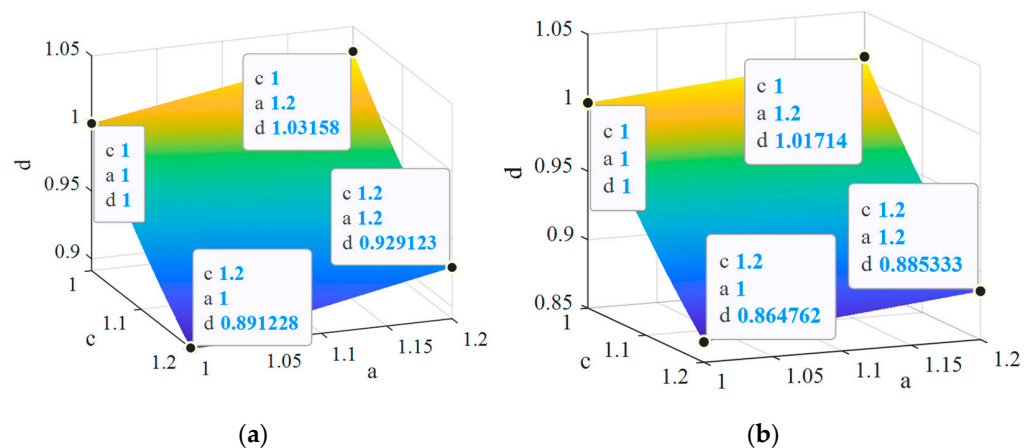


**Figure 9.** Solution of  $d$  after simplifying in different output resistances: (a)  $R_o = 2 \Omega$ ,  $P_o = 800 \text{ W}$ ; (b)  $R_o = 4 \Omega$ ,  $P_o = 400 \text{ W}$ .

Based on Equation (30), this paper designs a dynamic hybrid compensator (DHC) for current sharing control of parallel PSFB; the block diagram is shown in Figure 11. The factors  $a$ ,  $c$  and  $\delta$  are hardware parameters of the system that need to be measured in advance and preset in the compensator; they do not change as the system runs. They are the known parameters. The only unknown element in the control process is the total output resistance:  $R_o$ . It can be calculated by the output voltage  $V_o$  and the current of both phases  $I_{o1}$  and  $I_{o2}$ . The master module is responsible for maintaining the output voltage. By combining the main module's phase shift duty cycle  $D_1$  and the calculated phase shift duty cycle compensation  $d$ , the slave module can adjust its own phase shift duty cycle,  $D_2$ ,

in real time to achieve two-phase current sharing control. The PI controller is used in DHC for further reduction of current sharing control errors.

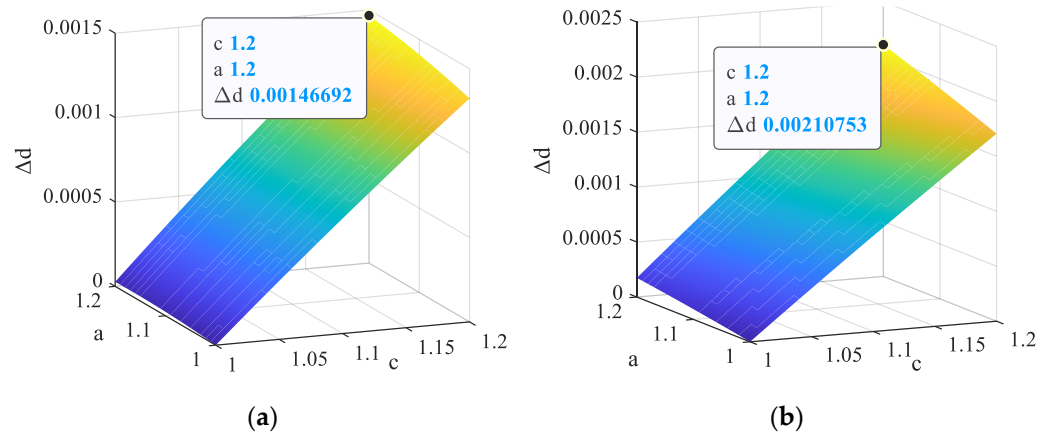


**Figure 10.** Error of  $d$  base on Equation (30) in different output resistances: (a)  $R_o = 2 \Omega, P_o = 800 \text{ W}$ ; (b)  $R_o = 4 \Omega, P_o = 400 \text{ W}$ .

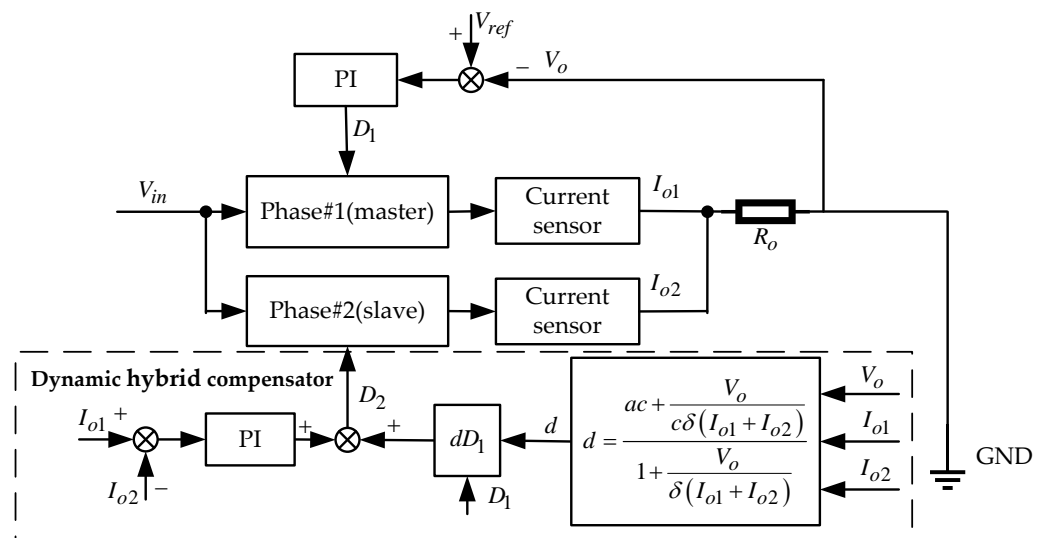


**Figure 11.** Block diagram of parallel PSFB with DHC.

#### 4. Simulation Result

In this section, MATLAB and Simulink simulation results for the influence of circuit component differences are analyzed. The circuit part and controller part of the simulation model are shown in Figures 12 and 13. In addition, the simulation of the parallel PSFB converter without current sharing and the system with the DHC controlling will be shown in the next section to further compare and validate the current sharing control performance.

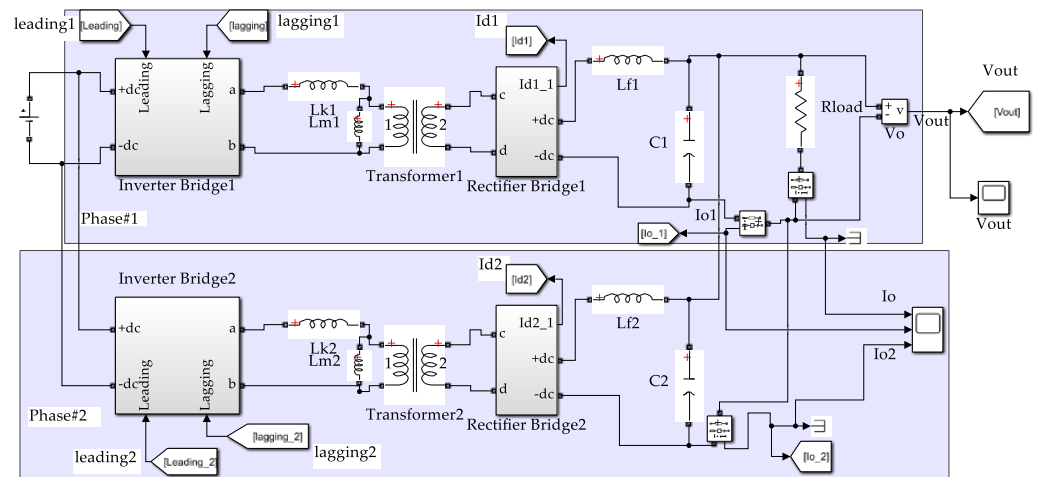


Figure 12. Circuit part of simulation model.

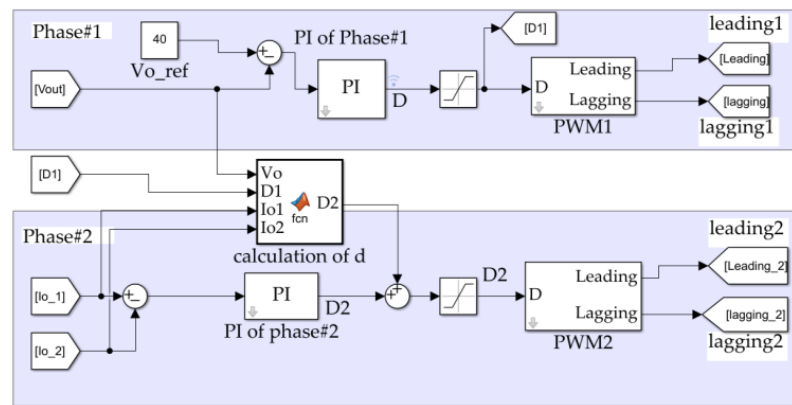


Figure 13. Controller part of simulation model.

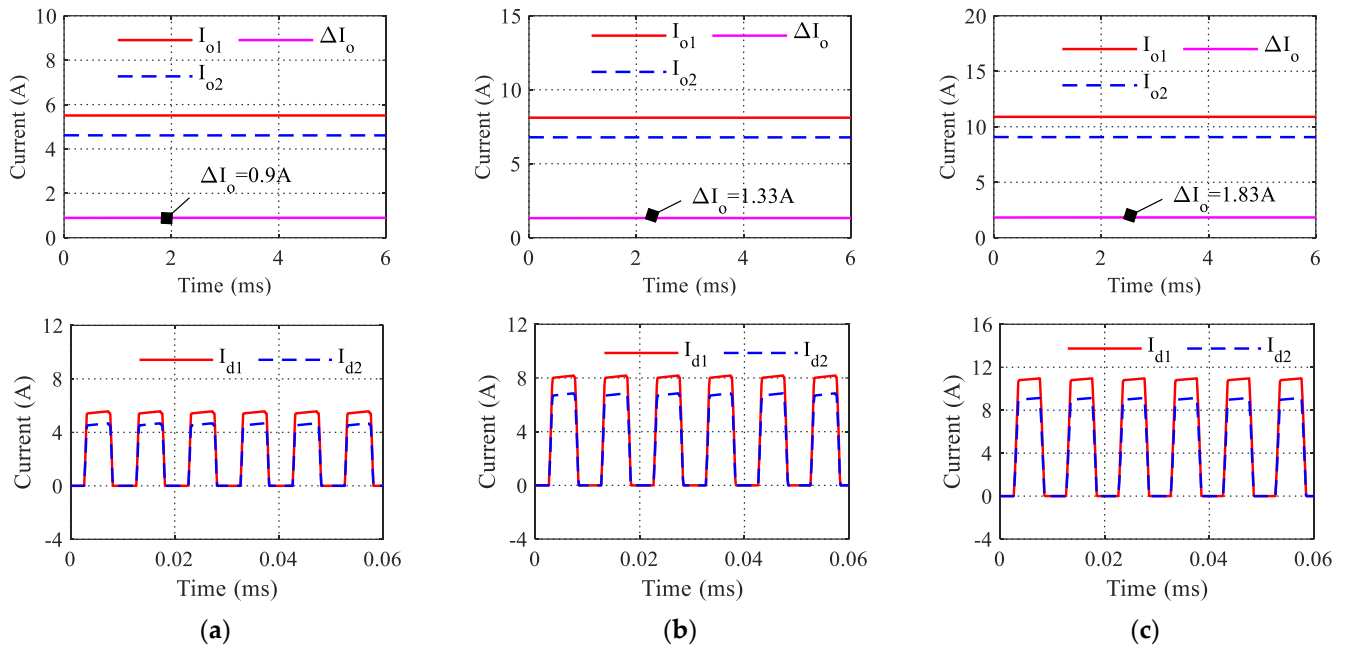
#### 4.1. Influence of Leakage Inductor Difference

Figure 14 shows the simulation result of the output current  $I_o$  and rectifier current  $I_d$  at the maximum leakage inductor difference ( $a = 1.2$ ).

Table 3 shows each phase's load current and the total load current. It can be observed from the simulation that the output current sharing error,  $\sigma_{load}$ , matches the calculation results. The diversity in current sharing error at different output power is not significant; the error  $\sigma_{load}$  is about 9%. The secondary diodes of phase #1 are subjected to more current stress.

Table 3. Data comparison of different output power when  $a = 1.2$ .

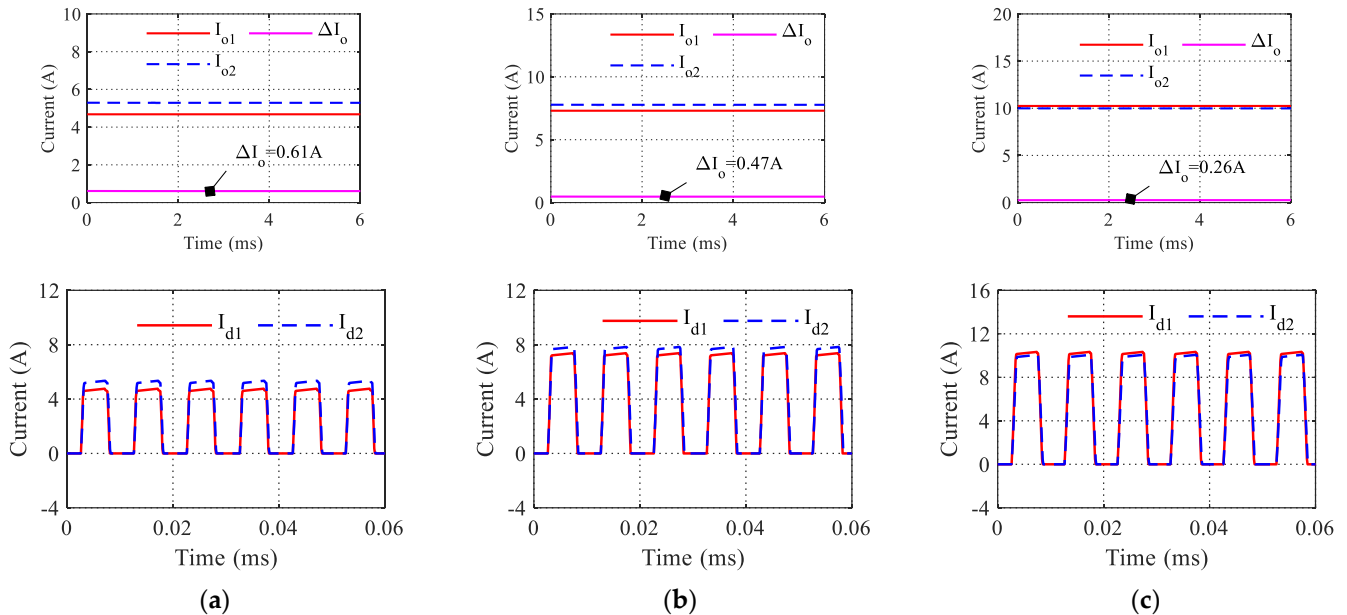
$P_o$	$I_o$	$I_{oi}$	$\Delta I_o$	$k_i$	$\sigma_{load}$
400 W	10.12 A	$I_{o1} = 5.5$ A $I_{o2} = 4.61$ A	$\Delta I_o = 0.9$ A	$k_1 = 0.543$ $k_2 = 0.456$	8.89%
600 W	14.89 A	$I_{o1} = 8.11$ A $I_{o2} = 6.78$ A	$\Delta I_o = 1.33$ A	$k_1 = 0.545$ $k_2 = 0.455$	8.93%
800 W	19.96 A	$I_{o1} = 10.89$ A $I_{o2} = 9.1$ A	$\Delta I_o = 1.83$ A	$k_1 = 0.546$ $k_2 = 0.456$	9.17%



**Figure 14.** Simulation result of output current and rectifier current in different output resistances when  $a = 1.2$ : (a)  $R_o = 4 \Omega$ ,  $P_o = 400 \text{ W}$ ; (b)  $R_o = 2.667 \Omega$ ,  $P_o = 600 \text{ W}$ ; (c)  $R_o = 2 \Omega$ ,  $P_o = 800 \text{ W}$ .

**Current Sharing Control Result When  $a = 1.2$**

Only using the calculation result  $d$ , the result of  $I_o$  and  $I_d$  when  $a = 1.2$  is shown in Figure 15.



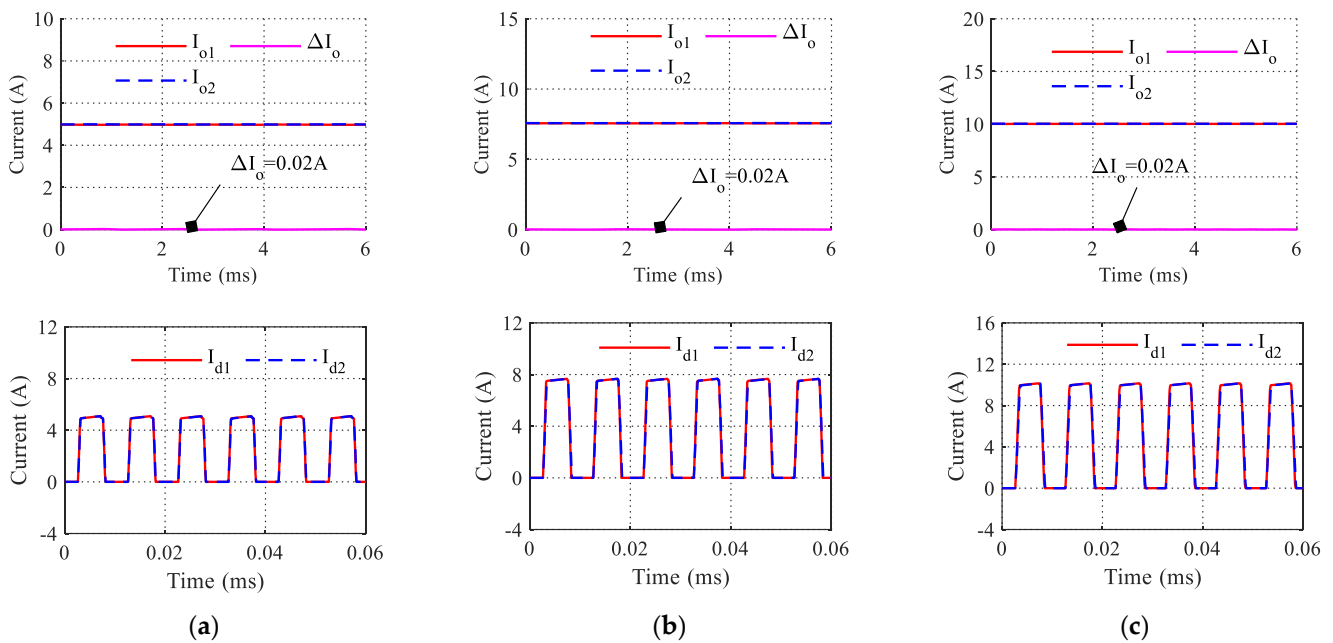
**Figure 15.** Simulation result of  $I_o$  and  $I_d$  in different  $P_o$  after using  $I_d$  calculation result when  $a = 1.2$ : (a)  $R_o = 4 \Omega$ ,  $P_o = 400 \text{ W}$ ; (b)  $R_o = 2.667 \Omega$ ,  $P_o = 600 \text{ W}$ ; (c)  $R_o = 2 \Omega$ ,  $P_o = 800 \text{ W}$ .

Table 4 shows the current sharing error,  $\sigma_{load}$ , after using the calculation result  $d$ . As the output power increases, the current sharing error decreases. Comparing the data in Tables 3 and 4, the phase-shift duty cycle compensation  $d$  can reduce the current imbalance caused by the leakage inductance difference, especially when operating at full load.

**Table 4.** Data comparison of different output power after only using calculation result when  $a = 1.2$ .

$P_o$	$I_o$	$I_{oi}$	$\Delta I_o$	$k_i$	$\sigma_{load}$
400 W	9.97 A	$I_{o1} = 4.68$ A $I_{o2} = 5.29$ A	$\Delta I_o = 0.61$ A	$k_1 = 0.47$ $k_2 = 0.53$	6.07%
600 W	15.08 A	$I_{o1} = 7.3$ A $I_{o2} = 7.78$ A	$\Delta I_o = 0.47$ A	$k_1 = 0.484$ $k_2 = 0.516$	3.12%
800 W	20.23 A	$I_{o1} = 10.24$ A $I_{o2} = 9.99$ A	$\Delta I_o = 0.26$ A	$k_1 = 0.506$ $k_2 = 0.494$	1.28%

The simulation result after using the proposed DHC current sharing control is shown in Figure 16 and Table 5. The current sharing error after using DHC is less than the error after only using the calculation  $d$  control. The errors are all less than 0.2%.



**Figure 16.** Simulation result of  $I_o$  and  $I_d$  in different  $P_o$  after using DHC when  $a = 1.2$ ; (a)  $R_o = 4 \Omega$ ,  $P_o = 400$  W; (b)  $R_o = 2.667 \Omega$ ,  $P_o = 600$  W; (c)  $R_o = 2 \Omega$ ,  $P_o = 800$  W.

**Table 5.** Data comparison of different output power after using DHC when  $a = 1.2$ .

$P_o$	$I_o$	$I_{oi}$	$\Delta I_o$	$k_i$	$\sigma_{load}$
400 W	9.97 A	$I_{o1} = 4.98$ A $I_{o2} = 4.99$ A	$\Delta I_o = 0.02$ A	$k_1 = 0.5$ $k_2 = 0.5$	0.2%
600 W	15.14 A	$I_{o1} = 7.57$ A $I_{o2} = 7.56$ A	$\Delta I_o = 0.02$ A	$k_1 = 0.5$ $k_2 = 0.5$	0.13%
800 W	20.07 A	$I_{o1} = 10.04$ A $I_{o2} = 10.03$ A	$\Delta I_o = 0.02$ A	$k_1 = 0.5$ $k_2 = 0.5$	0.1%

4.2. Influence of Filter Inductor Difference

Figure 17 and Table 6 show the simulation data of the output current  $I_o$  and rectifier current  $I_d$  at the maximum filter inductor difference ( $b = 1.2$ ).

The biggest current sharing error,  $\sigma_{load,r} = 0.06\%$ . Compared to the other parameters, the current imbalance caused by filter inductor difference can be ignored.

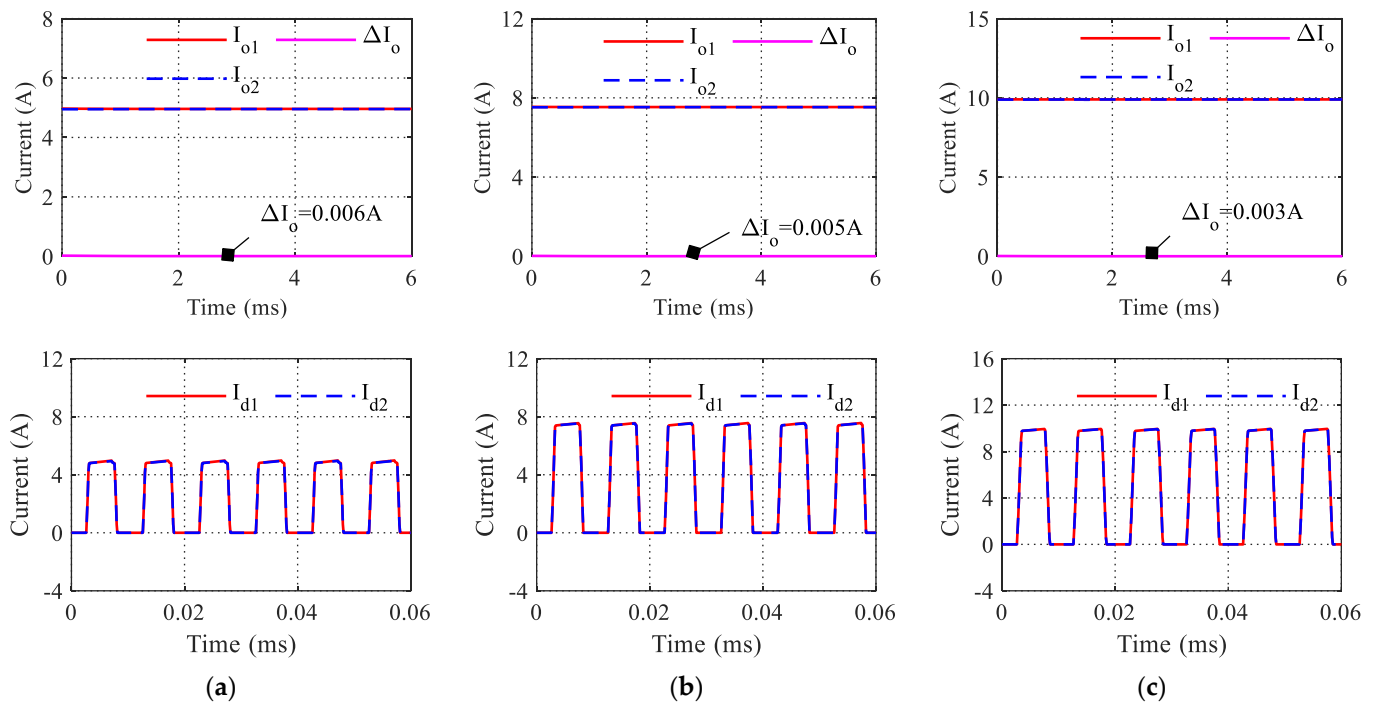


**Figure 17.** Simulation result of  $I_o$  and  $I_d$  in different  $P_o$  when  $b = 1.2$ : (a)  $R_o = 4 \Omega$ ,  $P_o = 400 \text{ W}$ ; (b)  $R_o = 2.667 \Omega$ ,  $P_o = 600 \text{ W}$ ; (c)  $R_o = 2 \Omega$ ,  $P_o = 800 \text{ W}$ .

**Table 6.** Data comparison of different output power when  $b = 1.2$ .

$P_o$	$I_o$	$I_{oi}$	$\Delta I_o$	$k_i$	$\sigma_{load}$
400 W	9.92 A	$I_{o1} = 4.96 \text{ A}$ $I_{o2} = 4.96 \text{ A}$	$\Delta I_o = 0.006 \text{ A}$	$k_1 = 0.5$ $k_2 = 0.5$	0.06%
600 W	15.06 A	$I_{o1} = 7.53 \text{ A}$ $I_{o2} = 7.53 \text{ A}$	$\Delta I_o = 0.005 \text{ A}$	$k_1 = 0.5$ $k_2 = 0.5$	0.03%
800 W	19.8 A	$I_{o1} = 9.89 \text{ A}$ $I_{o2} = 9.91 \text{ A}$	$\Delta I_o = 0.003 \text{ A}$	$k_1 = 0.5$ $k_2 = 0.5$	0.02%

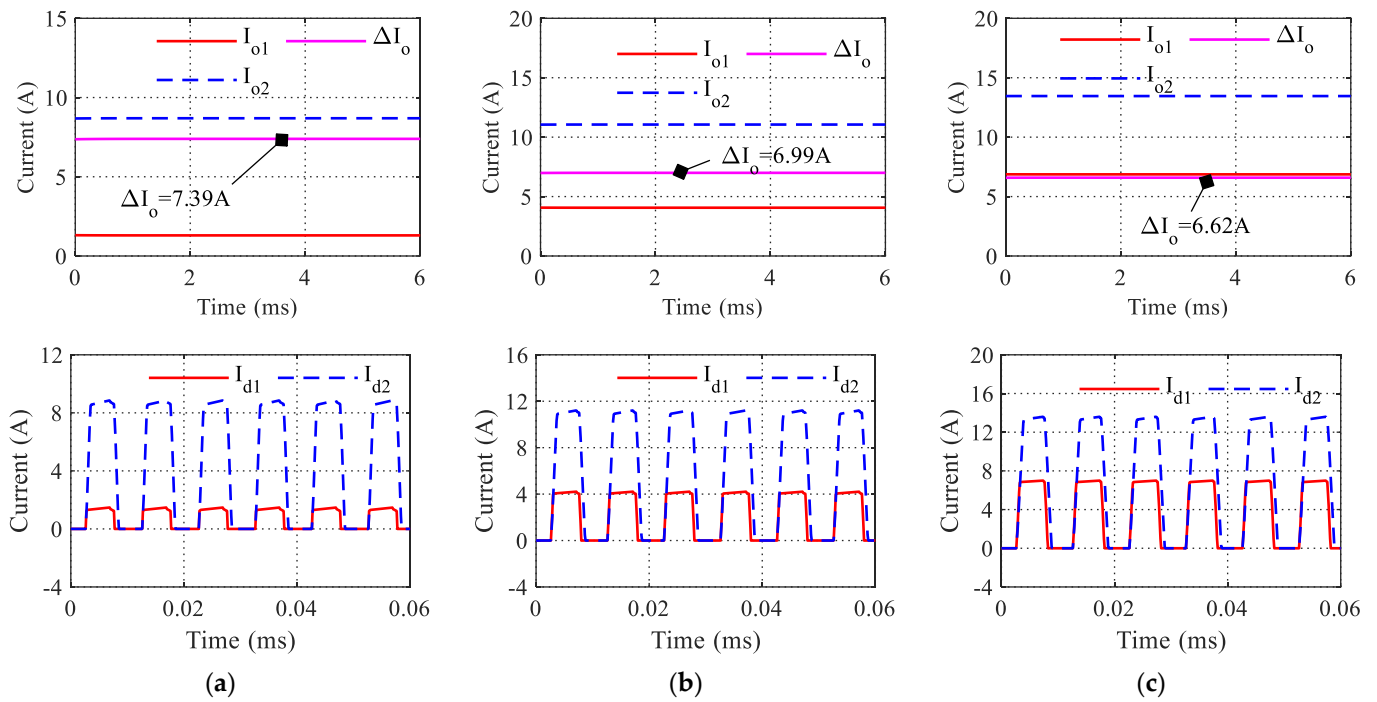
#### 4.3. Influence of Transformer Ratio Difference

Figure 18 displays the  $I_o$  and  $I_d$  without current sharing control simulation results at the highest transformer ratio difference ( $c = 1.2$ ).

Table 7 shows the current sharing error  $\sigma_{load}$  without using the current sharing control when  $c = 1.2$ . The transformer ratio difference is the most important factor causing output current imbalance among the three parameters. In the worst case where  $R_o = 4 \Omega$  and  $P_o = 400 \text{ W}$ , the load current sharing error  $\sigma_{load}$  reaches 73.98%. When  $k_1 = 0.13$ , phase #1 only outputs 13% of the total power and phase #2 supplies 87% of the total power. The secondary diodes of phase #2 are subjected more current stress.

**Table 7.** Data comparison of different output power without current sharing control when  $c = 1.2$ .

$P_o$	$I_o$	$I_{oi}$	$\Delta I_o$	$k_i$	$\sigma_{load}$
400 W	10 A	$I_{o1} = 1.3 \text{ A}$ $I_{o2} = 8.69 \text{ A}$	$\Delta I_o = 7.39 \text{ A}$	$k_1 = 0.13$ $k_2 = 0.87$	73.98%
600 W	15.11 A	$I_{o1} = 4.06 \text{ A}$ $I_{o2} = 11.05 \text{ A}$	$\Delta I_o = 6.99 \text{ A}$	$k_1 = 0.269$ $k_2 = 0.731$	46.26%
800 W	20.3 A	$I_{o1} = 6.84 \text{ A}$ $I_{o2} = 13.46 \text{ A}$	$\Delta I_o = 6.62 \text{ A}$	$k_1 = 0.337$ $k_2 = 0.663$	32.61%



**Figure 18.** Simulation result of  $I_o$  and  $I_d$  in different  $P_o$  without current sharing control when  $c = 1.2$ : (a)  $R_o = 4 \Omega$ ,  $P_o = 400 \text{ W}$ ; (b)  $R_o = 2.667 \Omega$ ,  $P_o = 600 \text{ W}$ ; (c)  $R_o = 2 \Omega$ ,  $P_o = 800 \text{ W}$ .

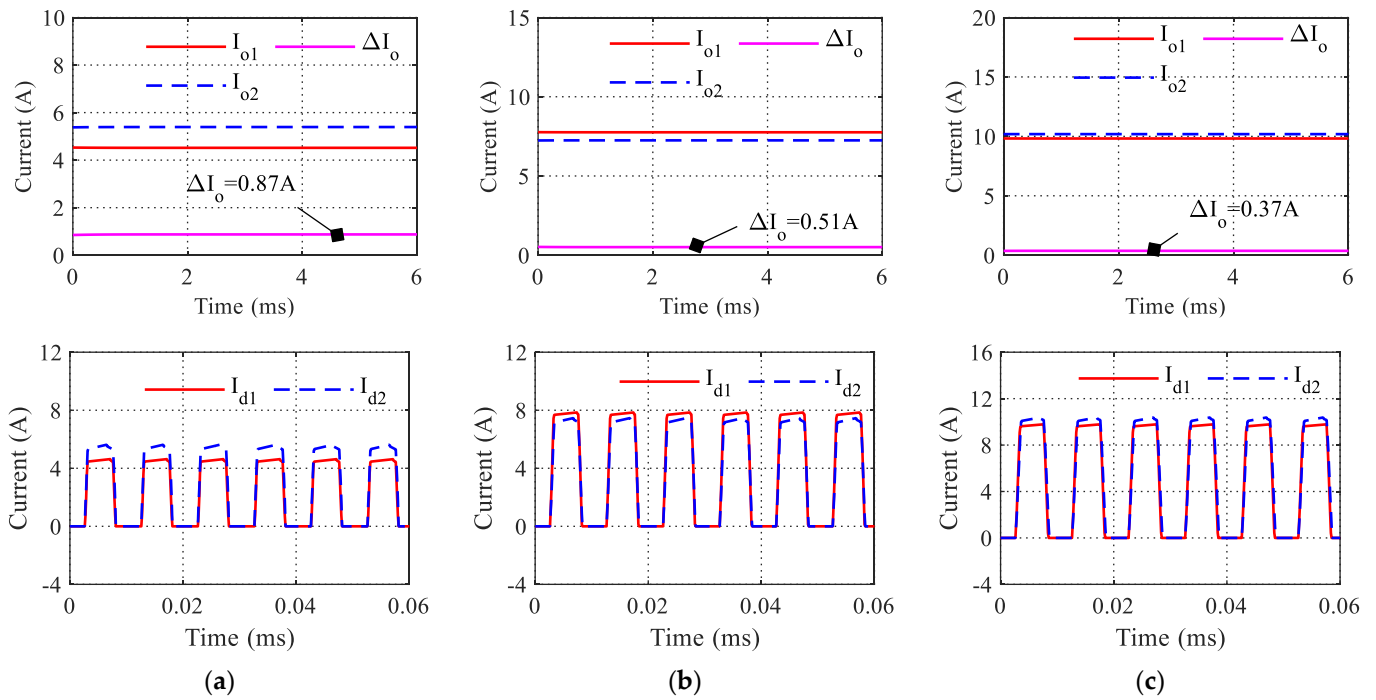
**Current Sharing Control Result when  $c = 1.2$**

Figure 19 and Table 8 show the simulation result after only using calculation  $d$ . It can be seen that, after using the current sharing control, the current sharing error decreases as the total output power increases. In the simulation, in the worst case, where  $R_o = 4 \Omega$  and  $P_o = 400 \text{ W}$ , the load current sharing error  $\sigma_{load} = 8.82\%$ . In the worst case, the load current sharing error  $\sigma_{load}$  reaches 73.98%. At the full output power case, where  $R_o = 2 \Omega$  and  $P_o = 800 \text{ W}$ , the load current sharing error  $\sigma_{load} = 1.84\%$ .

**Table 8.** Data comparison of different output power after only using calculation result when  $c = 1.2$ .

$P_o$	$I_o$	$I_{oi}$	$\Delta I_o$	$k_i$	$\sigma_{load}$
400 W	9.91 A	$I_{o1} = 4.52 \text{ A}$ $I_{o2} = 5.39 \text{ A}$	$\Delta I_o = 0.87 \text{ A}$	$k_1 = 0.456$ $k_2 = 0.544$	8.82%
600 W	15.01 A	$I_{o1} = 7.76 \text{ A}$ $I_{o2} = 7.25 \text{ A}$	$\Delta I_o = 0.51 \text{ A}$	$k_1 = 0.517$ $k_2 = 0.483$	3.41%
800 W	20.01 A	$I_{o1} = 9.82 \text{ A}$ $I_{o2} = 10.19 \text{ A}$	$\Delta I_o = 0.37 \text{ A}$	$k_1 = 0.491$ $k_2 = 0.509$	1.84%

The simulation result where  $c = 1.2$  after using the DHC is shown in Figure 20 and Table 9. The  $\sigma_{load}$  of the parallel PSFB system after using DHC current sharing control can be further reduced when compared with only using the calculated  $d$ . At the half output power case, with the current error  $\Delta I_o = 0.1 \text{ A}$ , each phase supplies almost half the power of the total output power.



**Figure 19.** Simulation result of  $I_o$  and  $I_d$  in different  $P_o$  after only using calculation result when  $c = 1.2$ : (a)  $R_o = 4\Omega, P_o = 400\text{ W}$ ; (b)  $R_o = 2.667\ \Omega, P_o = 600\text{ W}$ ; (c)  $R_o = 2\ \Omega, P_o = 800\text{ W}$ .

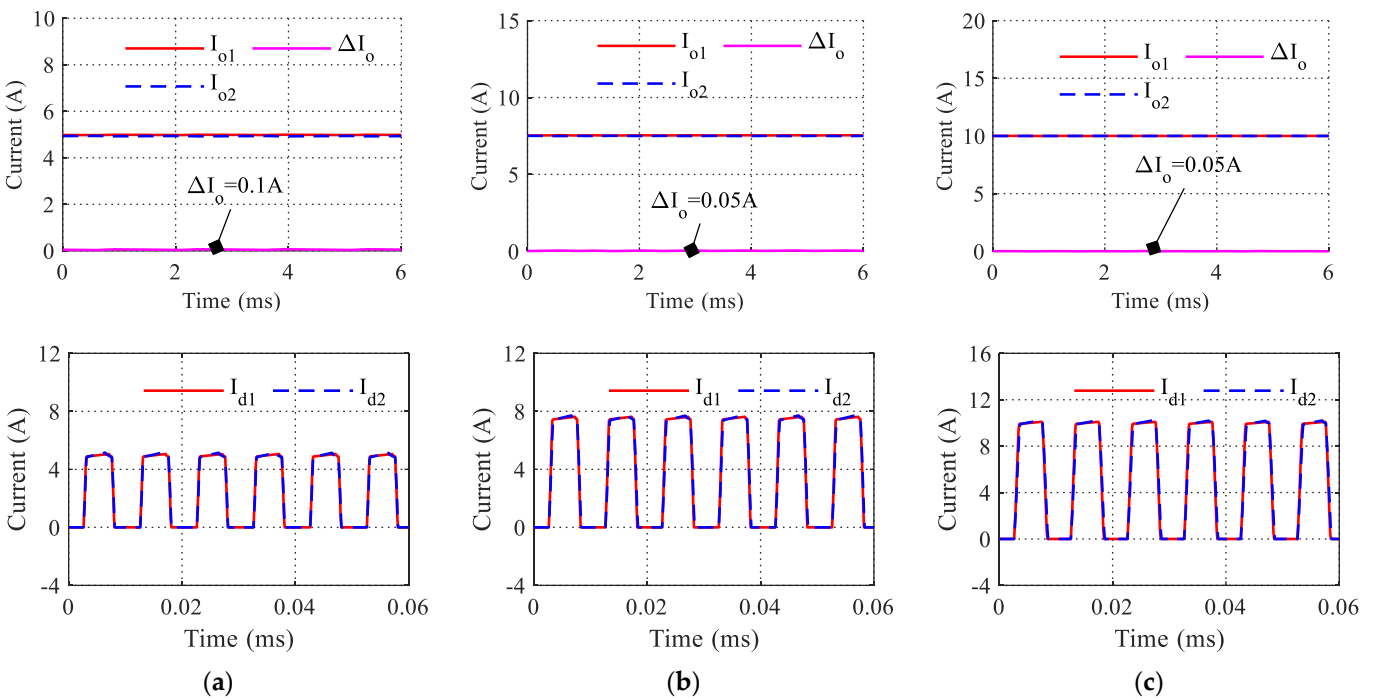


**Figure 20.** Simulation result of  $I_o$  and  $I_d$  in different  $P_o$  after using DHC when  $c = 1.2$ : (a)  $R_o = 4\ \Omega, P_o = 400\text{ W}$ ; (b)  $R_o = 2.667\ \Omega, P_o = 600\text{ W}$ ; (c)  $R_o = 2\ \Omega, P_o = 800\text{ W}$ .

**Table 9.** Data comparison of different output power after using DHC when  $c = 1.2$ .

$P_o$	$I_o$	$I_{oi}$	$\Delta I_o$	$k_i$	$\sigma_{load}$
400 W	9.92 A	$I_{o1} = 4.91$ A $I_{o2} = 5.01$ A	$\Delta I_o = 0.1$ A	$k_1 = 0.495$ $k_2 = 0.505$	1.01%
600 W	15.04 A	$I_{o1} = 7.51$ A $I_{o2} = 7.52$ A	$\Delta I_o = 0.05$ A	$k_1 = 0.499$ $k_2 = 0.5$	0.33%
800 W	20 A	$I_{o1} = 10.02$ A $I_{o2} = 9.98$ A	$\Delta I_o = 0.05$ A	$k_1 = 0.501$ $k_2 = 0.499$	0.25%

**5. Experiment Result**

An 800 W prototype using a two-phase PSFB converter is designed and fabricated to verify the feasibility of the proposed dynamic hybrid compensator and to demonstrate its effectiveness. The circuit schematic is shown in Figure 4. The design of the circuit component parameters is based on the traditional design method of a single-phase PSFB converter. The testing bench and prototype of the two-phase PSFB converter are shown in Figure 21. The prototype component values are shown in Table 10 [26,27]. MOSFET IRFP360PBF from Infineon are used as the converter switches. The TMS320F280049 from TI is adopted in the control module. The models of the oscilloscope, load and the source are Tektronix MSO54, ITECH IT6018B-800-75 and EA-PS 9500-90, respectively.

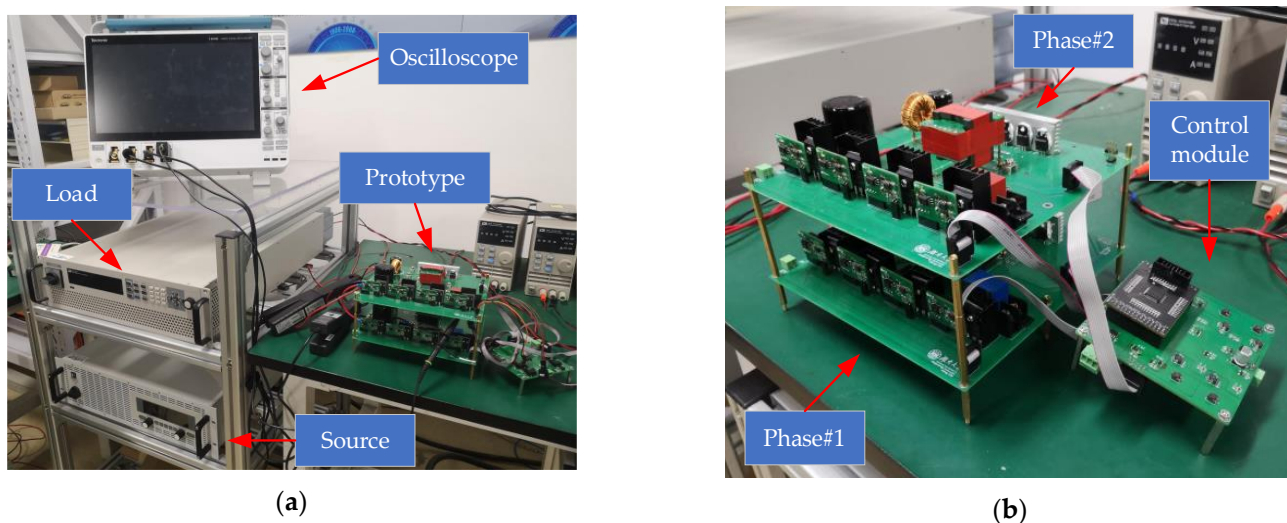


**Figure 21.** Testing bench and prototype of two-phase PSFB converter: (a) testing bench; (b) prototype.

**Table 10.** Prototype circuit component values.

Parameter	Value
Rated input voltage $V_{in}$	200 V
Rated output voltage $V_o$	40 V
Full load current $I_o$	10 A $\times$ 2
Rated output power $P_o$	400 W $\times$ 2
Leakage inductor $L_r$	31.29 $\mu$ H (phase#1), 27.59 $\mu$ H (phase#2)
Filter inductor $L_f$	237.69 $\mu$ H (phase#1), 265.86 $\mu$ H (phase#2)
Transformer ratio 1/n	24:6(phase#1), 24:7(phase#2)
Switch frequency	100 kHz

Define the phase #1 as the master module and the phase #2 as the salve module. The leakage inductor difference factor  $a = 0.882$ , the filter inductor difference factor  $b = 1.12$ , and

the transformer ratio difference factor  $c = 1.168$ . All the parameter differences are basically consistent with the maximum value set by the calculation and simulation in this paper.

Figure 22 shows the experiment result of the two-phase PSFB converter without current sharing control at 400 W, 600 W and 800 W total output power. Table 11 shows each phase output load current, power ratio  $k$  and current sharing error. As shown in the figure, the phase #2 supplies almost all the load current and the phase #1 supplies very little of the total output power. As the data in Table 11 show, at the worst case where  $R_o = 4 \Omega$  and  $P_o = 400$  W, the phase #2 supplies the 94.2% total power and the current sharing error  $\sigma_{load} = 88.39\%$ . The difference between the experimental and simulation results is due to the coexistence of  $a$  and  $c$ .

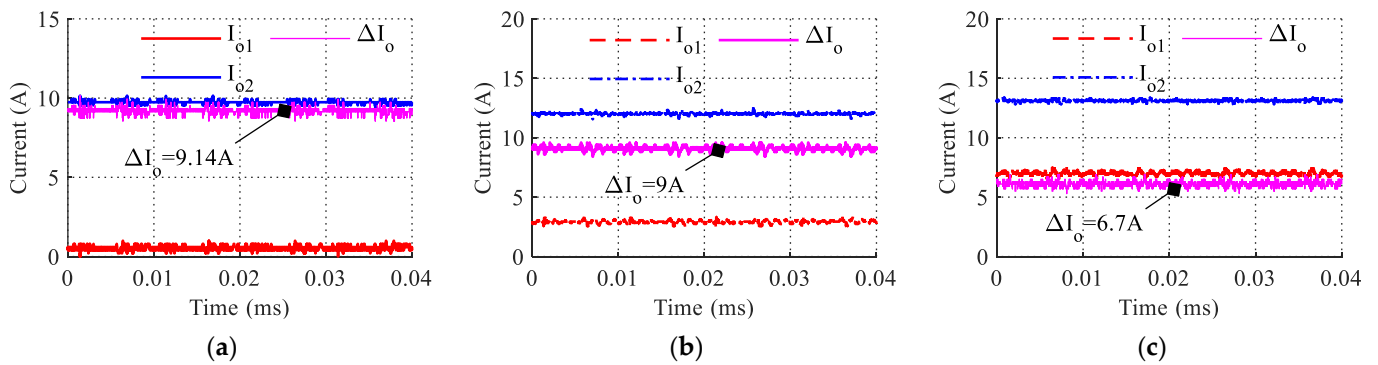


**Figure 22.** Experimental result of output current without current sharing control in different  $P_o$ : (a)  $R_o = 4 \Omega$ ,  $P_o = 400$  W; (b)  $R_o = 2.667 \Omega$ ,  $P_o = 600$  W; (c)  $R_o = 2 \Omega$ ,  $P_o = 800$  W.

**Table 11.** Experimental data without current sharing control in different output power.

$P_o$	$I_o$	$I_{oi}$	$\Delta I_o$	$k_i$	$\sigma_{load}$
400 W	10.34 A	$I_{o1} = 0.6$ A $I_{o2} = 9.74$ A	$\Delta I_o = 9.14$ A	$k_1 = 0.058$ $k_2 = 0.942$	88.39%
600 W	14.88 A	$I_{o1} = 2.94$ A $I_{o2} = 11.94$ A	$\Delta I_o = 9$ A	$k_1 = 0.198$ $k_2 = 0.802$	60.48%
800 W	20.5 A	$I_{o1} = 6.9$ A $I_{o2} = 13.6$ A	$\Delta I_o = 6.7$ A	$k_1 = 0.337$ $k_2 = 0.663$	32.68%

Figure 23 and Table 12 show the experiment result of the two-phase PSFB converter after only using calculation phase-shift duty cycle compensation  $d$  to reduce the error of current sharing control at 400 W, 600 W and 800 W total output power.

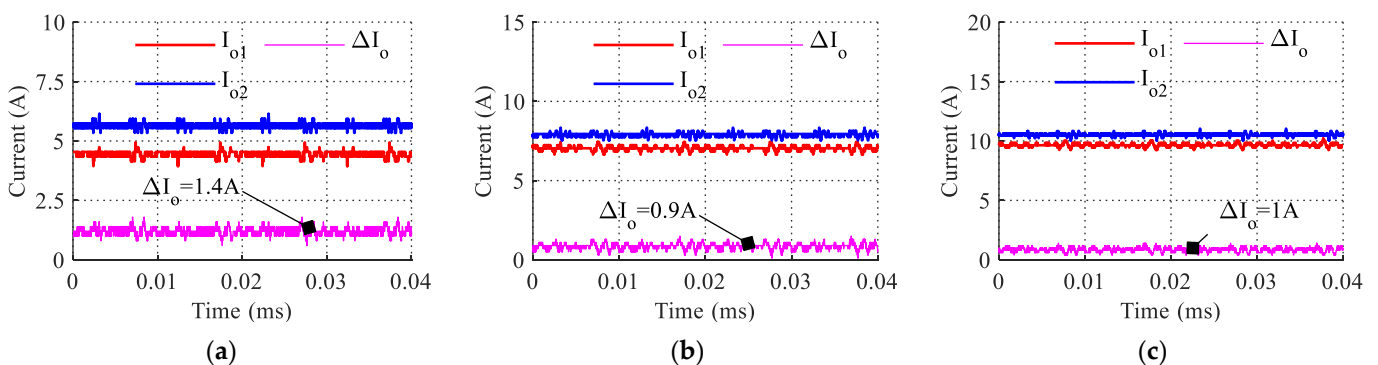


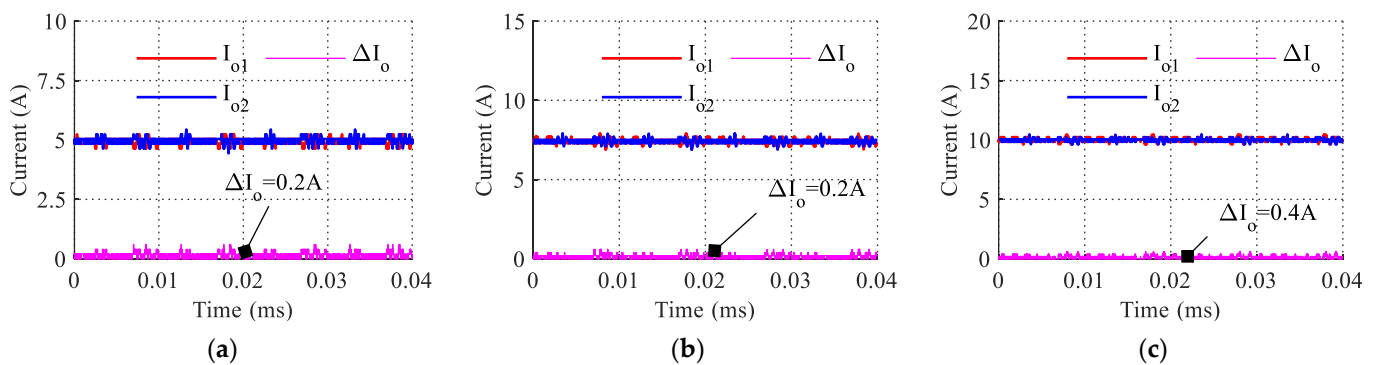
**Figure 23.** Experimental result of output current after only using calculation compensation: (a)  $R_o = 4 \Omega$ ,  $P_o = 400$  W; (b)  $R_o = 2.667 \Omega$ ,  $P_o = 600$  W; (c)  $R_o = 2 \Omega$ ,  $P_o = 800$  W.

**Table 12.** Experimental data after only using calculation compensation.

$P_o$	$I_o$	$I_{oi}$	$\Delta I_o$	$k_i$	$\sigma_{load}$
400 W	10.08 A	$I_{o1} = 4.34$ A $I_{o2} = 5.74$ A	$\Delta I_o = 1.4$ A	$k_1 = 0.431$ $k_2 = 0.569$	13.9%
600 W	14.98 A	$I_{o1} = 7.04$ A $I_{o2} = 7.94$ A	$\Delta I_o = 0.9$ A	$k_1 = 0.47$ $k_2 = 0.53$	6.01%
800 W	20.28 A	$I_{o1} = 9.64$ A $I_{o2} = 10.64$ A	$\Delta I_o = 1$ A	$k_1 = 0.475$ $k_2 = 0.525$	4.93%

In the worst case, the phase #1 provides 43.1% output power and the current sharing error  $\sigma_{load} = 13.9\%$ . Compared with Table 11, the current imbalance is improved.

The experimental current data of two phases after using the DHC current sharing control are shown in Figure 24 and Table 13. The output current sharing error  $\sigma_{load}$  are 1.98% in 400 W, 1.33% in 600 W and 1.99% in 800 W. The current sharing control performance of DHC is better than only using the calculation compensation, especially in the half output power case. The current sharing error is less than 2%, which is significantly decreased than in the without current sharing case. The comparison of the dynamic performance between the proposed DHC control than the conventional PI control is shown in Figure 25. Although the steady-state errors are similar between the DHC control and the PI control, the dynamic response time of the DHC control is 1.7 ms faster than the PI control, showing a 36.2% improvement.

**Figure 24.** Experimental result of output current after using DHC: (a)  $R_o = 4 \Omega$ ,  $P_o = 400$  W; (b)  $R_o = 2.667 \Omega$ ,  $P_o = 600$  W; (c)  $R_o = 2 \Omega$ ,  $P_o = 800$  W.**Table 13.** Experimental data after using DHC.

$P_o$	$I_o$	$I_{oi}$	$\Delta I_o$	$k_i$	$\sigma_{load}$
400 W	10.08 A	$I_{o1} = 4.94$ A $I_{o2} = 5.14$ A	$\Delta I_o = 0.2$ A	$k_1 = 0.49$ $k_2 = 0.501$	1.98%
600 W	15 A	$I_{o1} = 7.4$ A $I_{o2} = 7.6$ A	$\Delta I_o = 0.2$ A	$k_1 = 0.493$ $k_2 = 0.507$	1.33%
800 W	20.08 A	$I_{o1} = 9.84$ A $I_{o2} = 10.24$ A	$\Delta I_o = 0.4$ A	$k_1 = 0.49$ $k_2 = 0.51$	1.99%

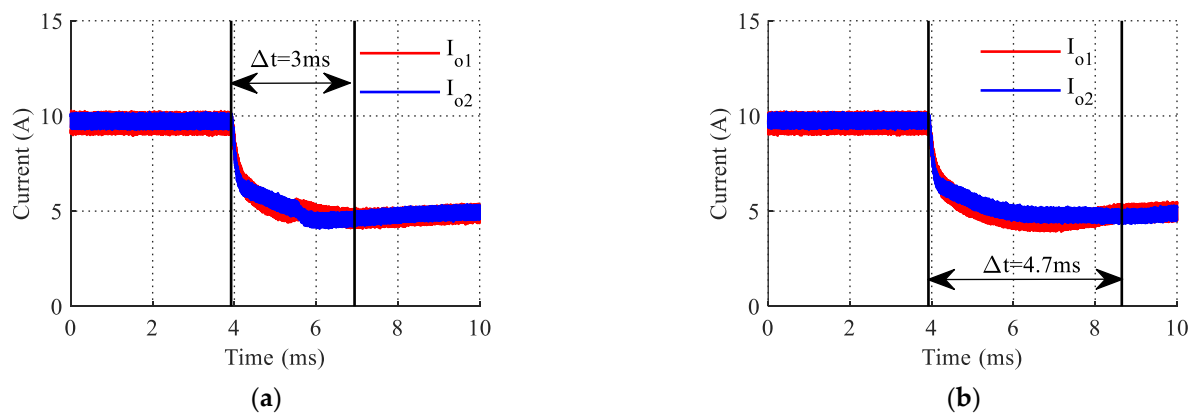


**Figure 25.** Experimental output current waveforms under 800 W–400 W load transient: (a) DHC control; (b) conventional PI control.

## 6. Conclusions

The IPOP-PSFB converter, that consists of multiple PSFB modules connected in parallel at the input and output, is a very attractive solution for expanding PSFB converter output power level application. Manufacturing differences make the output current different between modules. Therefore, it is to ensure that each module output current is shared evenly.

This paper proposes a mathematical model of an IPOP-PSFB system and a new dynamic hybrid compensator current sharing control method for the multiphase PSFB converter. The following conclusions can be drawn from the study:

- i. The influence of circuit elements on the performance of the current sharing control is analyzed and it is found that the leakage inductor difference and the transformer ratio difference are the main factors in current sharing control errors.
- ii. A dynamic phase-shift duty cycle compensator cooperating with a PI controller is proposed to achieve the output balance of current sharing control. The simulation analysis results indicate that the proposed strategy can significantly decrease the current sharing error, even with a component difference lower than 20%. A further experimental test on a prototype 800 W two-phase PSFB converter shows that the proposed DHC control can reduce the current sharing error to less than 2% under both half and full load conditions.

However, the method proposed in this paper still has a shortcoming: the hardware parameters of the system need to be measured in advance and preset in DHC. This increases the operational complexity. More work is required to identify the error coefficients of parallel PSFB converter and improve the method.

**Author Contributions:** Conceptualization, B.G., K.L. and H.L.; Methodology, B.G., K.L. and H.L.; Software, B.G.; Resources, K.L.; Writing—original draft, B.G.; Writing—review & editing, B.G., K.L., J.W., J.Z., S.T., C.H. and H.W. All authors have read and agreed to the published version of the manuscript.

**Funding:** This research was funded by National Natural Science Foundation of China, grant number 51877075.

**Data Availability Statement:** Not applicable.

**Conflicts of Interest:** The authors declare no conflict of interest.

## References

1. Chen, W.; Ruan, X.; Yan, H.; Tse, C.K. DC/DC Conversion Systems Consisting of Multiple Converter Modules: Stability, Control, and Experimental Verifications. *IEEE Trans. Power Electron.* **2009**, *24*, 1463–1474. [[CrossRef](#)]
2. Duan, J.; Zhang, D.; Wang, L.; Zhou, Z.; Gu, Y. Active Voltage Sharing Module for Input-Series Connected Modular DC/DC Converters. *IEEE Trans. Power Electron.* **2020**, *35*, 5987–6000. [[CrossRef](#)]

3. Bui, D.-V.; Cha, H.; Nguyen, C.V. Asymmetrical PWM Scheme Eliminating Duty Cycle Limitation in Input-Parallel Output-Series DC–DC Converter. *IEEE Trans. Power Electron.* **2022**, *37*, 2485–2490. [[CrossRef](#)]
4. Xinbo, R.; Wu, C.; Lulu, C.; Tse, C.K.; Hong, Y.; Tao, Z. Control Strategy for Input-Series–Output-Parallel Converters. *IEEE Trans. Ind. Electron.* **2009**, *56*, 1174–1185. [[CrossRef](#)]
5. Ma, D.; Chen, W.; Ruan, X. A Review of Voltage/Current Sharing Techniques for Series–Parallel-Connected Modular Power Conversion Systems. *IEEE Trans. Power Electron.* **2020**, *35*, 12383–12400. [[CrossRef](#)]
6. Shi, J.; Liu, T.; Cheng, J.; He, X. Automatic Current Sharing of an Input-Parallel Output-Parallel (IPOP)-Connected DC–DC Converter System With Chain-Connected Rectifiers. *IEEE Trans. Power Electron.* **2015**, *30*, 2997–3016. [[CrossRef](#)]
7. Lin, Y.; Wang, Y.; Wang, S.; Li, H. Sensorless current estimation and sharing in multiphase input-parallel output-parallel DC-DC converters. In Proceedings of the 2015 IEEE 2nd International Future Energy Electronics Conference (IFEEEC), Taipei, Taiwan, 1–4 November 2015; pp. 1–6. [[CrossRef](#)]
8. Foley, R.F.; Kavanagh, R.C.; Egan, M.G. Sensorless Current Estimation and Sharing in Multiphase Buck Converters. *IEEE Trans. Power Electron.* **2012**, *27*, 2936–2946. [[CrossRef](#)]
9. Kelly, A. Current Share in Multiphase DC–DC Converters Using Digital Filtering Techniques. *IEEE Trans. Power Electron.* **2009**, *24*, 212–220. [[CrossRef](#)]
10. Hwu, K.I.; Chen, Y.H. Current Sharing Control Strategy Based on Phase Link. *IEEE Trans. Ind. Electron.* **2012**, *59*, 701–713. [[CrossRef](#)]
11. Ahmad, U.; Cha, H.; Naseem, N. Integrated Current Balancing Transformer Based Input-Parallel Output-Parallel LLC Resonant Converter Modules. *IEEE Trans. Power Electron.* **2021**, *36*, 5278–5289. [[CrossRef](#)]
12. Giri, R.; Choudhary, V.; Ayyanar, R.; Mohan, N. Common-duty-ratio control of input-series connected modular DC-DC converters with active input voltage and load-current sharing. *IEEE Trans. Ind. Appl.* **2006**, *42*, 1101–1111. [[CrossRef](#)]
13. Shi, J.; Zhou, L.; He, X. Common-Duty-Ratio Control of Input-Parallel Output-Parallel (IPOP) Connected DC–DC Converter Modules With Automatic Sharing of Currents. *IEEE Trans. Power Electron.* **2012**, *27*, 3277–3291. [[CrossRef](#)]
14. Wang, Y.; Wang, F.; Lin, Y.; Hao, T. Sensorless parameter estimation and current-sharing strategy in two-phase and multiphase IPOP DAB DC–DC converters. *IET Power Electron.* **2018**, *11*, 1135–1142. [[CrossRef](#)]
15. Wang, H.; Chen, Y.; Liu, Y.-F.; Afsharian, J.; Yang, Z. A Passive Current Sharing Method With Common Inductor Multiphase LLC Resonant Converter. *IEEE Trans. Power Electron.* **2017**, *32*, 6994–7010. [[CrossRef](#)]
16. Wang, H.; Chen, Y.; Qiu, Y.; Fang, P.; Zhang, Y.; Wang, L.; Liu, Y.-F.; Afsharian, J.; Yang, Z. Common Capacitor Multiphase LLC Converter With Passive Current Sharing Ability. *IEEE Trans. Power Electron.* **2018**, *33*, 370–387. [[CrossRef](#)]
17. Wang, H.; Chen, Y.; Liu, Y.-F.; Liu, S. Automatic current-sharing method for multi-phase LLC resonant converter. In Proceedings of the 2016 IEEE 8th International Power Electronics and Motion Control Conference (IPEMC-ECCE Asia), Hefei, China, 22–26 May 2016; pp. 3198–3205. [[CrossRef](#)]
18. Wang, H.; Chen, Y.; Liu, Y.-F. A Passive-Impedance-Matching Technology to Achieve Automatic Current Sharing for a Multiphase Resonant Converter. *IEEE Trans. Power Electron.* **2017**, *32*, 9191–9209. [[CrossRef](#)]
19. Abu-Qahouq, J.A. Analysis and Design of N-Phase Current-Sharing Autotuning Controller. *IEEE Trans. Power Electron.* **2010**, *25*, 1641–1651. [[CrossRef](#)]
20. Zhang, J.M.; Xie, X.G.; Wu, X.K.; Zhaoming, Q. Comparison study of phase-shifted full bridge ZVS converters. In Proceedings of the IEEE 35th Annual Power Electronics Specialists Conference, Aachen, Germany, 20–25 June 2004; pp. 533–539. [[CrossRef](#)]
21. Hua, G.; Lee, F.C.; Jovanovic, M.M. An improved full-bridge zero-voltage-switched PWM converter using a saturable inductor. *IEEE Trans. Power Electron.* **1993**, *8*, 530–534. [[CrossRef](#)]
22. Xinbo, R.; Fuxin, L. An improved ZVS PWM full-bridge converter with clamping diodes. In Proceedings of the IEEE 35th Annual Power Electronics Specialists Conference, Aachen, Germany, 20–25 June 2004; pp. 1476–1481. [[CrossRef](#)]
23. You, J.; Cheng, L.; Fu, B.; Deng, M. Analysis and Control of Input-Parallel Output-Series Based Combined DC/DC Converter With Modified Connection in Output Filter Circuit. *IEEE Access* **2019**, *7*, 58264–58276. [[CrossRef](#)]
24. Huang, L.; Zhou, Y.; Huang, J.; Zeng, J.; Chen, G. Analysis and Design of ZVZCS Full-Bridge Converter With Reduced Components for Input-Series-Output-Parallel Application. *IEEE Trans. Ind. Electron.* **2021**, *68*, 6806–6817. [[CrossRef](#)]
25. Shi, J.; Luo, J.; He, X. Common-Duty-Ratio Control of Input-Series Output-Parallel Connected Phase-shift Full-Bridge DC–DC Converter Modules. *IEEE Trans. Power Electron.* **2011**, *26*, 3318–3329. [[CrossRef](#)]
26. Badstuebner, U.; Biela, J.; Kolar, J.W. Design of an 99%-efficient, 5 kW, phase-shift PWM DC-DC converter for telecom applications. In Proceedings of the 2010 Twenty-Fifth Annual IEEE Applied Power Electronics Conference and Exposition (APEC), Palm Springs, CA, USA, 21–25 February 2010; pp. 773–780. [[CrossRef](#)]
27. Escudero, M.; Kutschak, M.-A.; Meneses, D.; Rodriguez, N.; Morales, D.P. A Practical Approach to the Design of a Highly Efficient PSFB DC-DC Converter for Server Applications. *Energies* **2019**, *12*, 3723. [[CrossRef](#)]

**Disclaimer/Publisher’s Note:** The statements, opinions and data contained in all publications are solely those of the individual author(s) and contributor(s) and not of MDPI and/or the editor(s). MDPI and/or the editor(s) disclaim responsibility for any injury to people or property resulting from any ideas, methods, instructions or products referred to in the content.